Nuclear Science and Techniques (2025) 36:144
https://doi.org/10.1007/s41365-025-01723-2

Multiple scattering effects in Glauber model descriptions of single-nucleon removal reactions

Rui-Ying Chen[1] · Dan-Yang Pang[1,2] · Cen-Xi Yuan[3] · Yi-Ping Xu[4] · Wen-Di Chen[1] · Wen-Long Hai[1] · Jing-Jing Yan[1] · Wei-Jia Kong[1]

Received: 15 October 2024 / Revised: 24 January 2025 / Accepted: 26 January 2025 / Published online: 4 June 2025

Abstract
The Glauber/eikonal model is a widely used tool for studying intermediate- and high-energy nuclear reactions. When calculating the Glauber/eikonal model phase shift functions, the optical limit approximation (OLA) is often used. The OLA neglects the multiple scattering of the constituent nucleons in the projectile and target nuclei. However, the nucleon–target version of the Glauber model (the NTG model) proposed by Abu-Ibrahim and Suzuki includes multiple scattering effects between the projectile nucleons and target nuclei. The NTG model was found to improve the description of the elastic scattering angular distributions and total reaction cross sections of some light heavy-ion systems with respect to the OLA. In this work, we study the single-nucleon removal reactions (SNRRs) induced by carbon isotopes on ^{12}C and ^{9}Be targets using both the NTG model and the OLA. Reduction factors (RFs) of the single-nucleon spectroscopic factors were obtained by comparing the experimental and theoretical SNRR cross sections. On average, the RFs obtained with the NTG model were smaller than those obtained using the OLA by 7.8%, in which the average difference in one-neutron removal was 10.6% and that in one-proton removal was 4.2%. However, the RFs were still strongly dependent on the neutron–proton asymmetry ΔS of the projectile nuclei, even when the NTG model was used.

Keywords Glauber model of nuclear reactions · Single-nucleon removal reactions · Spectroscopic factors

1 Introduction

The measurements and theoretical analyses of single-nucleon removal reactions are of great value in studies on the single-particle strengths of atomic nuclei, which are quantitatively represented by spectroscopic factors (SFs) [1]. It is well known that the SFs extracted from (e, e′p) and single-nucleon transfer reactions are found to be 30%–50% smaller than those predicted by the configuration–interaction shell model (CISM) [2, 3]. Such a reduction or quenching of SFs, represented by the quenching factors R_s, is supposed to originate from the limited model spaces and insufficient treatment of the nucleon–nucleon correlations in the traditional CISM [4, 5]. Unlike the results from (e, e′p) reactions, from single-nucleon transfer reactions [6–8], and from (p, 2p) and (p, pn) reactions [2, 3, 9, 10], where the R_s values of different nuclei are nearly constant, the quenching factors from intermediate energy single-nucleon removal reactions are found to have an almost linear relationship with the proton–neutron asymmetry of the atomic nuclei, ΔS ($\Delta S = S_p - S_n$ for proton removal and $\Delta S = S_n - S_p$ for neutron removal with S_n and S_p being the neutron and proton separation energies in the ground states of the projectile nuclei, respectively) [11, 12]. For cases when ΔS is larger than approximately 20 MeV, which corresponds to the

This work was financially supported by the National Key R&D Program of China (No. 2023YFA1606702) and the National Natural Science Foundation of China (Nos. U2067205 and 12205098).

✉ Dan-Yang Pang
dypang@buaa.edu.cn

[1] School of Physics, Beihang University, Beijing 100191, China

[2] Beijing Key Laboratory of Advanced Nuclear Materials and Physics, Beihang University, Beijing 100191, China

[3] Sino-French Institute of Nuclear Engineering and Technology, Sun Yat-Sen University, Zhuhai 519082, China

[4] School of Nuclear Science and Engineering, North China Electric Power University, Beijing 102206, China

removal of strongly bound nucleons, the R_s values decrease to approximately 0.3; however, when ΔS is smaller than approximately − 20 MeV, which corresponds to the removal of weakly bound nucleons, the R_s values are close to unity. The reasons for such a clear linear dependence observed in the results of the intermediate-energy single-nucleon removal reactions remain unknown. Because most single-nucleon removal reactions are analyzed using the Glauber model, the validity of the eikonal/Glauber model [11–13] has been questioned [14].

Owing to its simplicity, the optical limit approximation (OLA) is often used in the eikonal/Glauber model analysis of intermediate- and high-energy nuclear reactions [13, 15–19]. Only the first-order term for the expansion of the full Glauber phase shift is considered in the OLA. Higher-order interactions, such as nucleon–nucleon multiple scattering processes, are neglected [20]. In Ref. [21], B. Abu-Ibrahim and Y. Suzuki found that although the Glauber model with the OLA can reasonably reproduce the total reaction cross sections of some stable ions on ^{9}Be, ^{12}C, and ^{27}Al targets, it failed to reproduce the reaction cross sections and elastic scattering angular distributions of unstable nuclei.

For this, they proposed calculating the projectile–target phase shifts using nucleon–target interactions in the Glauber model calculations. This so-called nucleon–target version of the Glauber model (NTG model) has been found to considerably improve the description of the reaction cross sections and elastic scattering angular distribution data [21–23]. However, to the best of our knowledge, application of the NTG model to the analysis of single-nucleon knockout reactions and its influence on the reduction factors of single-particle strengths have not yet been studied. In this study, we investigated the extent to which the R_s values of single-nucleon knockout reactions change when the NTG model is used instead of the usual OLA. Because the NTG model includes multiple scattering effects in the phase shift functions of the colliding systems with respect to the OLA, we expect this work to provide information about the extent to which multiple scattering effects affect the description of single-nucleon removal reactions using the Glauber model.

This paper is organized as follows: The NTG model and the OLA of the Glauber model are briefly introduced in Sect. 2. The results of our calculations are given in Sect. 3, which include (1) an examination of the NTG model regarding its reproduction of the elastic scattering and total reaction cross-sectional data; the cases studied are the angular distributions of ^{12}C elastic scattering from a carbon target at incident energies from 30 to 200 MeV/u and the ^{12}C+^{12}C total reaction cross sections from 20 to 1000 MeV/u; (2) detailed study of the NTG model on single-nucleon removal at different incident energies; the case studied here is the ^{9}Be(^{19}C,^{18} C)X reaction; and (3) the effects of the NTG model on the reduction factors of the single-particle strengths. The cases studied are single-nucleon removal cross sections of carbon isotopes $^{9,10,12-20}$C on ^{9}Be and carbon targets within 43–250 MeV/u incident energies. The range of ΔS covered in these reactions is from −26.6 to 20.1 MeV. All results are compared with those of the OLA calculations to elucidate the influence of multiple scattering effects on these reactions. Finally, the conclusions are presented in Sect. 4.

2 The NTG model and the OLA

The NTG model was introduced in Refs. [21, 22]. Details of its formulae can be found in Ref. [20]. For convenience, we have summarized the necessary ones here. Let us start with the phase shift function of a nucleon–target system χ_{NT}, which is defined in the Glauber model framework as [20]:

$$e^{i\chi_{NT}(\boldsymbol{b})} = \left\langle \Phi_0^T \middle| \prod_{j=1}^{A_T} \left[1 - \Gamma_{NN}(\boldsymbol{b} - \boldsymbol{t}_j)\right] \middle| \Phi_0^T \right\rangle, \tag{1}$$

where $\boldsymbol{b}$ is the impact factor vector; $\boldsymbol{t}_j$ is the projection vector of the position of the jth nucleon in the target nucleus on the x-y plane (the beam direction is the z-axis); Γ_{NN} is the nucleon–nucleon (NN) profile function, which is the Fourier transform of the NN scattering amplitude; and $|\Phi_0\rangle$ is the wave function of the target nucleus, which has a mass number A_T. When an independent particle model wave function is used, which is usually assumed in the Glauber model calculations, the density of the target nucleus can be written as [20]

$$|\Phi_0^T(\boldsymbol{r}_1, \boldsymbol{r}_2, \ldots, \boldsymbol{r}_{A_T})|^2 = \prod_{j=1}^{A_T} n_j(\boldsymbol{r}_j), \tag{2}$$

where $n_j(\boldsymbol{r}_j)$ denotes the normalized density distribution of the jth nucleon in the target nucleus. The nucleon density distribution is then

$$\rho_T(\boldsymbol{r}) = \sum_{j=1}^{A_T} n_j(\boldsymbol{r}). \tag{3}$$

Using an uncorrelated wave function that satisfies Eq. (2), the nucleon–target phase shift function has the form [20]:

$$e^{i\chi_{NT}(\boldsymbol{b})} = \prod_{j=1}^{A_T} \left[1 - \int \mathrm{d}\boldsymbol{r} n_j(\boldsymbol{r}) \Gamma_{NN}(\boldsymbol{b} - \boldsymbol{t})\right], \tag{4}$$

where $\boldsymbol{t}$ is the projection of $\boldsymbol{r}$ on the x-y plane. When the range of the NN interaction is smaller than the radius of the target nucleus, which is satisfied in most cases, integral

$\int \mathrm{d}\boldsymbol{r} n_j(\boldsymbol{r})\Gamma_{\mathrm{NN}}(\boldsymbol{b}-\boldsymbol{t})$ is less than unity [20]. Then, the following approximation can be obtained [20]:

$$1-\int \mathrm{d}\boldsymbol{r} n_j(\boldsymbol{r})\Gamma_{\mathrm{NN}}(\boldsymbol{b}-\boldsymbol{t}) \approx e^{-\int \mathrm{d}\boldsymbol{r} n_j(\boldsymbol{r})\Gamma_{\mathrm{NN}}(\boldsymbol{b}-\boldsymbol{t})}. \tag{5}$$

Then, we obtained the nucleon–target phase shift of the OLA [20]:

$$\begin{aligned} e^{i\chi_{\mathrm{NT}}^{\mathrm{OLA}}(\boldsymbol{b})} &= \prod_{j=1}^{A_{\mathrm{T}}} \exp\left[-\int \mathrm{d}\boldsymbol{r} n_j(\boldsymbol{r})\Gamma_{\mathrm{NN}}(\boldsymbol{b}-\boldsymbol{t})\right] \\ &= \exp\left[-\sum_{j=1}^{A_{\mathrm{T}}}\int \mathrm{d}\boldsymbol{r} n_j(\boldsymbol{r})\Gamma_{\mathrm{NN}}(\boldsymbol{b}-\boldsymbol{t})\right] \\ &= \exp\left[-\int \mathrm{d}\boldsymbol{r}\rho_{\mathrm{T}}(\boldsymbol{r})\Gamma_{\mathrm{NN}}(\boldsymbol{b}-\boldsymbol{t})\right]. \end{aligned} \tag{6}$$

This results in the following nucleon–nucleus phase shift function using the OLA:

$$\chi_{\mathrm{NT}}^{\mathrm{OLA}}(\boldsymbol{b}) = i\int d\boldsymbol{r}\rho_{\mathrm{T}}(\boldsymbol{r})\Gamma_{\mathrm{NN}}(\boldsymbol{b}-\boldsymbol{t}). \tag{7}$$

Note that in Eqs. (1) and (4), multiple scattering terms appear through the cumulant expansion of the phase shift functions. However, after applying the approximation in Eq. (5) in Eq. (4), the resulting nucleon–nucleus phase shift with the OLA in Eq. (7) no longer contains multiple scattering terms [24].

Similar to the nucleon–nucleus case in Eq. (1), the nucleus–nucleus phase shift function, $\chi_{\mathrm{PT}}(\boldsymbol{b})$, for a composite projectile and target nucleus is [20]

$$\mathrm{e}^{i\chi_{\mathrm{PT}}(\boldsymbol{b})} = \left\langle \Phi_0^{\mathrm{P}}\Phi_0^{\mathrm{T}}\left|\prod_{i=1}^{A_{\mathrm{P}}}\prod_{j=1}^{A_{\mathrm{T}}}[1-\Gamma_{\mathrm{NN}}(\boldsymbol{b}+\boldsymbol{s}_i-\boldsymbol{t}_j)]\right|\Phi_0^{\mathrm{P}}\Phi_0^{\mathrm{T}}\right\rangle, \tag{8}$$

where Φ_0^{P} is the many-body wave function of the projectile (with mass number A_{P}) in its ground state. The integrals are over the coordinates of all nucleons i and j in the projectile and target nuclei, whose coordinates are $\boldsymbol{r}_i$ and $\boldsymbol{r}_j$, respectively. $\boldsymbol{s}_i$ and $\boldsymbol{t}_j$ are projections on the x-y plane. The nucleus–nucleus phase shift in this equation contains contributions from single collisions and all-order multiple scattering among the constituent nucleons in the projectile and target nuclei. Equation (8) is cumbersome to evaluate directly, although it is possible. Therefore, the optical limit approximation is typically used, and the phase shift function with this approximation is [20]

$$\chi_{\mathrm{PT}}^{\mathrm{OLA}}(\boldsymbol{b}) = i\int d\boldsymbol{r}_{\mathrm{P}}\rho_{\mathrm{P}}(\boldsymbol{r}_{\mathrm{P}})\int d\boldsymbol{r}_{\mathrm{T}}\rho_{\mathrm{T}}(\boldsymbol{r}_{\mathrm{T}})\Gamma_{\mathrm{NN}}(\boldsymbol{b}+\boldsymbol{s}-\boldsymbol{t}), \tag{9}$$

where ρ_{P} and ρ_{T} are the nucleon density distributions of the projectile and target nuclei, respectively, and $\boldsymbol{r}_{\mathrm{P}}$ and $\boldsymbol{r}_{\mathrm{T}}$ are the positions of their constituent nucleons, whose projections on the x-y plane are $\boldsymbol{s}$ and $\boldsymbol{t}$, respectively. As in the nucleon–nucleus case in Eq. (7), only a single NN collision contributes to the phase shift. The contributions from multiple scatterings are missing, which could be recovered to some extent by the nucleon–target version of the Glauber model (the NTG model) proposed by Abu-Ibrahim and Suzuki [20–23].

The idea of the NTG model is to replace $\langle\Phi_0^{\mathrm{T}}|\prod_{j\in\mathrm{T}}[1-\Gamma_{\mathrm{NN}}(\boldsymbol{b}+\boldsymbol{s}_i-\boldsymbol{t}_j)]|\Phi_0^{\mathrm{T}}\rangle$ for each nucleon i in the projectile in Eq. (8) by

$$\begin{aligned} &\left\langle \Phi_0^{\mathrm{T}}\left|\prod_{j=1}^{A_{\mathrm{T}}}[1-\Gamma_{\mathrm{NN}}(\boldsymbol{b}+\boldsymbol{s}_i-\boldsymbol{t}_j)]\right|\Phi_0^{\mathrm{T}}\right\rangle \\ &\quad\equiv 1-\Gamma_{\mathrm{NT}}(\boldsymbol{b}+\boldsymbol{s}_i), \end{aligned} \tag{10}$$

where $\Gamma_{\mathrm{NT}}(\boldsymbol{b}+\boldsymbol{s}_i)$ is the profile function of its collision with the target nucleus. The nucleus–nucleus phase shift takes the following form [20]:

$$\mathrm{e}^{i\chi_{\mathrm{PT}}^{\mathrm{NTG}}(\boldsymbol{b})} = \left\langle \Phi_0^{\mathrm{P}}\left|\prod_{i=1}^{A_{\mathrm{P}}}\left[1-\Gamma_{\mathrm{NT}}(\boldsymbol{b}+\boldsymbol{s}_i)\right]\right|\Phi_0^{\mathrm{P}}\right\rangle. \tag{11}$$

This model is referred to as the NTG model. Following the same procedure used to obtain Eq. (7), the phase shift of the projectile–target system with the NTG model is

$$\chi_{\mathrm{PT}}^{\mathrm{NTG}}(\boldsymbol{b}) = i\int \mathrm{d}\boldsymbol{r}\rho_{\mathrm{P}}(\boldsymbol{r})\Gamma_{\mathrm{NT}}(\boldsymbol{b}+\boldsymbol{s}), \tag{12}$$

and the nucleon–target profile function Γ_{NT} is

$$\begin{aligned} &\Gamma_{\mathrm{NT}}(\boldsymbol{b}+\boldsymbol{s}_i) \\ &\quad= 1-\left\langle \Phi_0^{\mathrm{T}}\left|\prod_{j=1}^{A_{\mathrm{T}}}[1-\Gamma_{\mathrm{NN}}(\boldsymbol{b}+\boldsymbol{s}_i-\boldsymbol{t}_j)]\right|\Phi_0^{\mathrm{T}}\right\rangle \\ &\quad= 1-\exp\left[-\int d\boldsymbol{r}_{\mathrm{T}}\rho_{\mathrm{T}}(\boldsymbol{r}_{\mathrm{T}})\Gamma_{\mathrm{NN}}(\boldsymbol{b}+\boldsymbol{s}-\boldsymbol{t})\right]. \end{aligned} \tag{13}$$

By substituting Γ_{NT} into Eq. (12), we obtain the nucleus–nucleus phase shift function of the NTG model:

$$\begin{aligned} \chi_{\mathrm{PT}}^{\mathrm{NTG}}(\boldsymbol{b}) &= i\int d\boldsymbol{r}_{\mathrm{P}}\rho_{\mathrm{P}}(\boldsymbol{r}_{\mathrm{P}}) \\ &\quad\times\left\{1-\exp\left[-\int d\boldsymbol{r}_{\mathrm{T}}\rho_{\mathrm{T}}(\boldsymbol{r}_{\mathrm{T}})\Gamma_{\mathrm{NN}}(\boldsymbol{b}+\boldsymbol{s}-\boldsymbol{t})\right]\right\}. \end{aligned} \tag{14}$$

The nucleus–nucleus phase shift of the NTG model contains multiple scattering effects other than the OLA, which can be seen by power expansion of the nucleon–target profile function of Eq. (13):

$$\Gamma_{\mathrm{NT}}(\boldsymbol{b}+\boldsymbol{s}_i) = \int \mathrm{d}\boldsymbol{r}_{\mathrm{T}}\rho_{\mathrm{T}}(\boldsymbol{r}_{\mathrm{T}})\Gamma_{\mathrm{NN}}(\boldsymbol{b}+\boldsymbol{s}-\boldsymbol{t}) - \frac{1}{2!}\left[\int \mathrm{d}\boldsymbol{r}_{\mathrm{T}}\rho_{\mathrm{T}}(\boldsymbol{r}_{\mathrm{T}})\Gamma_{\mathrm{NN}}(\boldsymbol{b}+\boldsymbol{s}-\boldsymbol{t})\right]^2 + \cdots . \quad (15)$$

The first term is contributed by single scattering of the projectile nucleon from the nucleons in the target nucleus. The second term and other terms represent the contributions from multiple NN scatterings [20]. If only the first term is used in Eq. (12), the NTG phase shift is reduced to that of the OLA in Eq. (9). Considering the higher-order terms in Eq. (15), phase shifts with the NTG model recover some multiple scattering effects that are missing from the OLA. However, the contributions from the multiple scattering processes included in this method are not identical to those in the full Glauber model in Eqs. (1) and (8) [25]. Nevertheless, as we will show in the next section, the NTG model could improve the description of the elastic scattering angular distributions, especially at low incident energies, and total reaction cross sections for the ^{12}C+^{12}C test case within a rather wide range of incident energies. In practice, a symmetrical version of the NTG phase shift is often calculated [21, 23] as

$$\chi^{\mathrm{NTG}}_{\mathrm{PT}}(\boldsymbol{b}) = \frac{i}{2}\int \mathrm{d}\boldsymbol{r}_{\mathrm{P}}\rho_{\mathrm{P}}(\boldsymbol{r}_{\mathrm{P}}) \left\{1-\exp\left[-\int \mathrm{d}\boldsymbol{r}_{\mathrm{T}}\rho_{\mathrm{T}}(\boldsymbol{r}_{\mathrm{T}})\Gamma_{\mathrm{NN}}(\boldsymbol{b}+\boldsymbol{s}-\boldsymbol{t})\right]\right\} + \frac{i}{2}\int \mathrm{d}\boldsymbol{r}_{\mathrm{T}}\rho_{\mathrm{T}}(\boldsymbol{r}_{\mathrm{T}}) \left\{1-\exp\left[-\int \mathrm{d}\boldsymbol{r}_{\mathrm{P}}\rho_{\mathrm{P}}(\boldsymbol{r}_{\mathrm{P}})\Gamma_{\mathrm{NN}}(\boldsymbol{b}+\boldsymbol{t}-\boldsymbol{s})\right]\right\}. \quad (16)$$

However, the phase shifts calculated using Eqs. (14) and (16) are often very close to each other [21, 22].

The profile function Γ_{NN} in both the OLA and NTG model calculations is parameterized in a Gaussian form:

$$\Gamma_{\mathrm{pN}}(\boldsymbol{b}) = \frac{1-i\alpha_{\mathrm{pN}}}{4\pi\beta_{\mathrm{pN}}}\sigma^{\mathrm{tot}}_{\mathrm{pN}}\exp\left(-\frac{\boldsymbol{b}^2}{2\beta_{\mathrm{pN}}}\right), \quad (17)$$

where the Γ_{NN} parameters $\sigma^{\mathrm{tot}}_{\mathrm{pN}}$, α_{pN}, and β_{pN} are the proton–nucleon total cross section, the ratio of the real to imaginary part of the p–N scattering amplitudes, and the corresponding slope parameter [26], respectively. Because of the lack of experimental data on neutron–neutron scattering, Γ_{pp} is commonly used instead of Γ_{NN}. In this study, $\sigma^{\mathrm{tot}}_{\mathrm{pN}}$ is obtained from Ref. [27], which is parameterized by fitting the experimental data from Ref. [28]; the α_{pN} parameters were taken from those tabulated in Ref. [26] for incident energies ranging from 100 to 2200 MeV/u. If the beam energy was lower than 100 MeV/u, we obtained the value corresponding to the lowest energy from the table. The finite-range slope parameters β_{pN} were taken to be 0.125 fm^2, in accordance with the systematic studies of single-nucleon removal reactions [13, 15, 29].

3 Comparisons between the NTG model and OLA in Glauber model calculations

In Ref. [30], T. Nagashisa and W. Horiuchi demonstrated the effectiveness of the NTG by comparing the description of the total reaction cross sections using the full Glauber model calculation, the NTG model, and the OLA for cases of ^{12,20,22}C on a ^{12}C target at various incident energies. In this work, our main purpose was to study how much the single-nucleon removal cross sections ($\sigma_{-1\mathrm{N}}$) change when the NTG model is used instead of the OLA. Before calculating $\sigma_{-1\mathrm{N}}$, we first compared our calculations for the elastic scattering angular distributions and total reaction cross sections with the experimental data and with the predictions of the OLA. The calculations were made for the ^{12}C+^{12}C system. Thus, we verified the effectiveness of the Γ_{NN} parameters used in our calculations, which were further used in the calculations of $\sigma_{-1\mathrm{N}}$. Single-nucleon removal reactions were calculated using a modified version of the computer code MOMDIS [31].

3.1 Elastic scattering angular distributions and total reaction cross sections

The angular distributions of ^{12}C elastic scattering from a ^{12}C target at 30, 85, 120, and 200 MeV/u were calculated with both the OLA and NTG model. The results are presented in Fig. 1 together with the experimental data. The dots are experimental data from Refs. [32, 33]. Clearly, the NTG improved the description of the ^{12}C+^{12}C elastic scattering considerably with respect to the OLA, especially when the incident energy was below approximately 100 MeV/u. This is expected because the multiple scattering effect, which is included in the NTG model but not in the OLA, is more important at low incident energies than at higher incident energies. Note that other corrections owing to, for instance, the antisymmetrization of the projectile and target wave-functions [34], Fermi motion of the nucleons in the colliding nuclei [35], and distortion of the trajectories [18] can also affect the low-energy cross sections. More complete calculations that consider these aspects together may be an interesting subject for the future.

A comparison of the NTG and OLA predictions and the total reaction cross sections of the ^{12}C+^{12}C system is shown in Fig. 2. The symbols represent experimental data from Ref. [36–43]. Again, we see that the results of the NTG

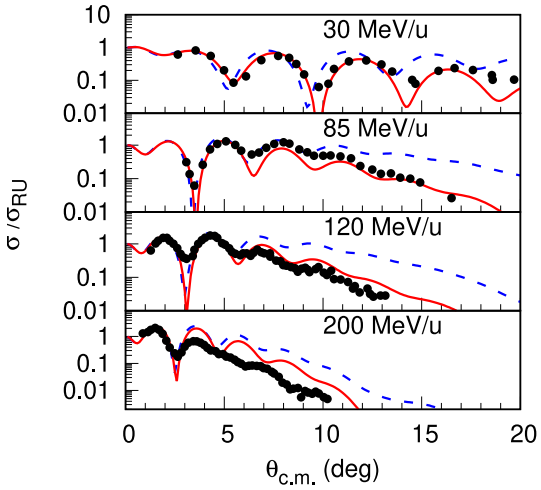

Fig. 1 (Color online) Elastic scattering angular distributions of ^{12}C on a carbon target at incident energies of 30, 85, 120, and 200 MeV/u. The red solid and blue dashed curves are results of Glauber model calculations with the NTG model and the OLA, respectively

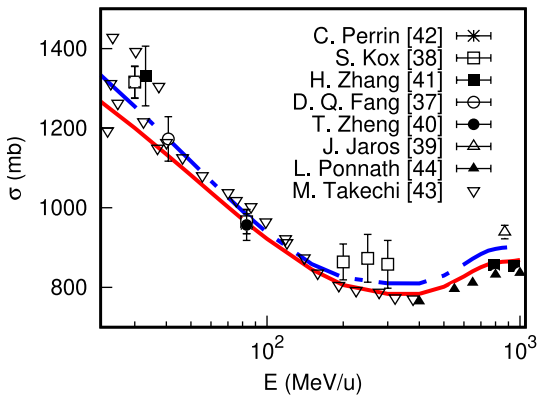

Fig. 2 (Color online) Reaction cross sections of ^{12}C on a carbon target. The red solid and blue dash–dotted curves are results of Glauber model calculations with the NTG model and the OLA, respectively

model are in better agreement with the experimental data than those of the OLA, especially for incident energies of several tens of MeV/u and above, where most of the one-nucleon removal cross-sectional data were measured [12]. In both elastic scattering and total reaction cross-sectional calculations, the proton and neutron density distributions of the ^{12}C nucleus are taken to be a Gaussian form with a root mean square radius of 2.32 fm [12], which is very close to the 2.33 ± 0.01 fm from elastic electron scattering data [44].

Note that the $\Gamma_{\rm NN}$ parameters are the same in both the NTG and OLA calculations. The only difference between these two methods is that the former introduces multiple scattering effects in the calculation of the eikonal phase functions. The improvement provided by the NTG model in the description of elastic scattering angular distributions and total reaction cross sections suggests that nuclear medium effects, such as the multiple scattering effect studied here, should be considered in the Glauber model description of nuclear reactions induced by heavy ions. In the following section, we study how the NTG model could affect the theoretical predictions of the single-neutron removal cross sections and single-particle strengths obtained from the experimental data.

3.2 Single-nucleon removal cross sections at different incident energies

In an inclusive single-nucleon removal reaction $A(a, b)X$, where only the core nucleus b ($A_b = A_a - 1$) is detected, two processes may occur: diffraction dissociation and stripping, which correspond to the escape of valence neutrons or their capture by the target nucleus, respectively. Within the Glauber model framework, their cross sections, $\sigma_{\rm sp}^{\rm dd}$ and $\sigma_{\rm sp}^{\rm str}$, respectively, are calculated by [45]

$$\sigma_{\rm sp}^{\rm dd} = \frac{1}{2j+1}\sum_m \int {\rm d}\boldsymbol{b}\Big[\Big\langle \psi_{nljm}\Big|\big|1 - S_{\rm v}S_{\rm c}\big|^2\Big|\psi_{nljm}\Big\rangle - \sum_{m'}\Big|\Big\langle \psi_{nljm'}\Big|\big(1 - S_{\rm v}S_{\rm c}\big)\Big|\psi_{nljm}\Big\rangle\Big|^2\Big], \tag{18}$$

and

$$\sigma_{\rm sp}^{\rm str} = \frac{1}{2j+1}\sum_m \int {\rm d}\boldsymbol{b}\big|S_{\rm c}\big|^2\times \Big\langle \psi_{nljm}\Big|\Big(1 - \big|S_{\rm v}\big|^2\Big)\Big|\psi_{nljm}\Big\rangle. \tag{19}$$

Here, $S_{\rm c} = e^{i\chi_{\rm cT}}$ and $S_{\rm v} = e^{i\chi_{\rm vT}}$ are the core–target and valence nucleon–target Smatrices, respectively. The valence nucleon–target phase shift function $\chi_{\rm vT}$ is calculated using Eq. (7), and the core–target phase shift function $\chi_{\rm cT}$ is calculated using Eq. (9) for the OLA and Eq. (16) for the NTG model; $\boldsymbol{b}$ is the impact factor vector of the projectile in the plane perpendicular to the beam direction; ψ_{nljm} is the single-particle wave function (SPWF) and n, l, and j are the principal, angular momentum, and total angular momentum numbers, respectively; and m is the projection of j. Equations (7, (9), (14), and (16) concern only nuclear phase shifts. The Coulomb phase shift must also be considered for charged particles [31]:

$$\chi_{\rm C} = 2\eta\ln(kb), \tag{20}$$

where $\eta = Z_1Z_2e^2\mu/\hbar^2k$ is the Sommerfeld parameter and Z_1 and Z_2 are the charge numbers of the two colliding particles, whose reduced mass is μ, and k is the wave number in the center-of-mass system. Single-particle wave functions are associated with the specific states of the core with spin I_b and

the composite nuclei with spin I_a by spectroscopic factors $(C^2S)_{I_aI_b,nlj}$. Therefore, the single-particle cross section of removal of a nucleon from the ground state of a projectile leaving the core nucleus in a specific state with the SPWF having quantum numbers nlj is

$$\sigma_{\rm sp}(I_aI_b,nlj) = \left(\frac{A}{A-1}\right)^N \left(C^2S\right)_{I_a,I_b,nlj} \times \left(\sigma_{\rm sp}^{\rm dd} + \sigma_{\rm sp}^{\rm str}\right), \quad (21)$$

where the $[A/(A-1)]^N$ factor represents the center-of-mass corrections to the spectroscopic factor C^2S [46] and $N = 2n + l$ is the number of oscillator quanta associated with the major shell of the removed particle (the minimum value of n is taken to be zero).

Experimentally, single-nucleon removal cross sections are usually measured inclusively, that is, only the core nucleus b is measured without discriminating its energy states. Correspondingly, theoretical calculations for these measurements should also include the contributions from all the bound excited states of the core nucleus b [13], which corresponds to a summation of all the single-particle cross sections associated with all possible single-particle wave functions:

$$\sigma_{-1\rm N}^{\rm th} = \sum_{nlj,I_b} \sigma_{\rm sp}(I_a,I_b,nlj). \quad (22)$$

To see how much difference the NTG model predicts in the single-nucleon removal cross sections with respect to the OLA, we study the (^{19}C,^{18}C) reaction on a ^{9}Be target at 64, 100, 200, and 400 MeV/u incident energies. The excited states of the ^{18}C nucleus, the associated single-particle wave functions, and their corresponding shell model predicted spectroscopic factors are taken to be the same as those in Ref. [15]. The single-particle wave functions are calculated with single-particle potentials of the Woods–Saxon forms with the depths adjusted to provide the experimental separation energies of the valence nucleon. The radius and diffuseness parameters were taken to be $r_0 = 1.25$ fm and $a = 0.7$ fm, respectively, the same as those used in Ref. [15]. The results are shown

Table 1 Single-neutron removal cross sections of ^{19}C on a beryllium target at incident energies of 64, 100, 200, and 400 MeV/u calculated using the NTG model, $\sigma_{-1\rm N}^{\rm NTG}$, and the OLA, $\sigma_{-1\rm N}^{\rm OLA}$. The state of the core nucleus and their corresponding single-nucleon spectroscopic factors are taken from Ref. [15]

$E_{\rm inc}$ (MeV/u)	E_x (MeV)	J^π	nlj	C^2S	$\sigma_{-1\rm N}^{\rm OLA}$ (mb)	$\sigma_{-1\rm N}^{\rm NTG}$ (mb)	$\sigma_{-1\rm N}^{\rm NTG}/\sigma_{-1\rm N}^{\rm OLA}$
64	0.000	0^+	$1s_{1/2}$	0.580	104.31	109.3	1.050
	2.144	2^+	$0d_{5/2}$	0.470	18.93	21.16	1.118
	3.639	2^+	$0d_{5/2}$	0.104	3.53	3.98	1.127
	3.988	0^+	$1s_{1/2}$	0.319	17.82	19.72	1.107
	4.915	3^+	$0d_{5/2}$	1.523	46.18	52.21	1.131
	4.975	2^+	$0d_{5/2}$	0.922	27.83	31.46	1.130
	Inclusive				218.42	237.83	1.089
100	0.000	0^+	$1s_{1/2}$	0.580	87.58	90.14	1.029
	2.144	2^+	$0d_{5/2}$	0.470	17.95	19.13	1.066
	3.639	2^+	$0d_{5/2}$	0.104	3.41	3.64	1.067
	3.988	0^+	$1s_{1/2}$	0.319	16.43	17.44	1.061
	4.915	3^+	$0d_{5/2}$	1.523	45.05	48.24	1.071
	4.975	2^+	$0d_{5/2}$	0.922	27.15	29.08	1.071
	Inclusive				197.57	207.67	1.051
200	0.000	0^+	$1s_{1/2}$	0.580	61.66	63.55	1.031
	2.144	2^+	$0d_{5/2}$	0.470	15.46	16.52	1.069
	3.639	2^+	$0d_{5/2}$	0.104	3.01	3.23	1.073
	3.988	0^+	$1s_{1/2}$	0.319	13.47	14.30	1.062
	4.915	3^+	$0d_{5/2}$	1.523	40.59	43.61	1.071
	4.975	2^+	$0d_{5/2}$	0.922	24.48	26.31	1.075
	Inclusive				158.67	167.52	1.056
400	0.000	0^+	$1s_{1/2}$	0.580	54.76	57.04	1.042
	2.144	2^+	$0d_{5/2}$	0.470	14.61	16.00	1.095
	3.639	2^+	$0d_{5/2}$	0.104	2.87	3.16	1.101
	3.988	0^+	$1s_{1/2}$	0.319	12.54	13.57	1.082
	4.915	3^+	$0d_{5/2}$	1.523	38.80	42.91	1.106
	4.975	2^+	$0d_{5/2}$	0.922	23.41	25.89	1.106
	Inclusive				146.99	158.57	1.079

in Table 1. Single-nucleon removal cross sections with the NTG model and OLA are denoted as σ_{-1N}^{NTG} and σ_{-1N}^{OLA}, respectively. Note that the σ_{-1N}^{OLA} values at 64 MeV/u agree well with those reported in Ref. [15]. The ratios of σ_{-1N}^{NTG} and σ_{-1N}^{OLA} are shown in Fig. 3.

It is interesting to note the following:

1. The one-nucleon removal cross sections calculated with the NTG model are larger than those calculated with the OLA within the whole energy range from 50 to 400 MeV/u.
2. Such differences are larger at incident energies smaller than approximately 100 MeV/u, almost constant around 100–200 MeV/u, and increase slightly when the incident energy is larger than approximately 200 MeV/u,
3. The differences are also more significant when the root mean square radius of the single-particle wave function is smaller, which means that the NTG model is especially important for one-neutron removal cross sections of a given reaction when the single nucleon is tightly bound.

The same was observed for the other nuclei examined in this study. The difference between the NTG model and the OLA is in the core–target S-matrix, S_c, only. However, as expressed in Eqs. (18) and (19), we cannot separate S_c from S_v and the single-particle wave functions when calculating the single-nucleon removal cross sections. Thus, we cannot show how the NTG model affects the σ_{-1N} values with respect to the OLA. In the following subsection, we discuss how the spectroscopic factors extracted from the experimental data and their reduction factors change when the NTG model is used instead of the OLA.

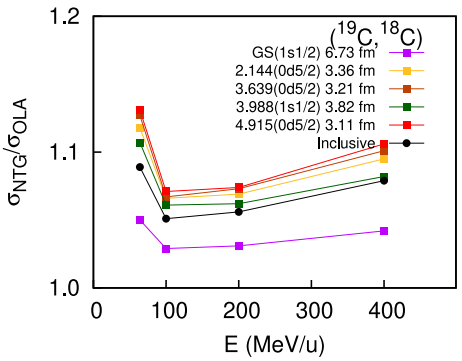

Fig. 3 (Color online) Ratios of the NTG and OLA predicted single-particle cross sections associated with different core states of the ^{9}Be(^{19}C,^{18}C)X reaction at incident energies 64, 100, 200, and 400 MeV/u. The black dots represent the results calculated with Eq. (22). The excitation energies of the core nucleus ^{18}C and the properties of their corresponding single-particle wave functions—their *nlj* values and root mean square radii—are also shown. The lines are to guide the eyes

3.3 Reduction factors of single-particle strengths

The spectroscopic factors in Eq. (22) are often obtained from configuration interaction shell model (CISM) calculations to determine one-nucleon removal cross sections. Owing to limited model spaces and insufficient treatment of nucleon–nucleon correlations, it is well known that CISM-predicted SFs are usually larger than the experimental ones. The reduction factors of the SFs, R_s, which are ratios of the experimental and theoretical SFs, are defined to quantify the differences. In the case of inclusive single-nucleon knockout reactions, the reduction factors are defined as the ratios between the experimental and theoretical cross sections [11, 12]:

$$R_s = \sigma_{-1N}^{exp}/\sigma_{-1N}^{th},$$

For nuclei with more than one set of available experimental data, the weighted mean of the R_s values for each measurement is used [47]:

$$\mathfrak{R} = \frac{\sum_i R_{si} w_i}{\sum_i w_i}, \tag{23}$$

where the weights are defined by the errors in the individual R_s values $(\Delta R_s)_i$:

$$w_i = \left[\frac{1}{\Delta R_{si}}\right]^2,$$

and the errors on average $\overline{R_s}$ are

$$\Delta\mathfrak{R} = \frac{1}{\sqrt{\sum_i w_i}}.$$

The effective neutron–proton asymmetry ΔS_{eff} is given by [15]

$$\Delta S_{eff} = S_n + \bar{E}_f - S_p, \text{ for neutron removal,}$$
$$\Delta S_{eff} = S_p + \bar{E}_f - S_n, \text{ for proton removal,}$$

where $\bar{E}_f$ is obtained by weighting the excitation energy E^* of each final state using the single-nucleon removal cross section of that state.

We analyzed a series of single-nucleon removal reaction data by using the method described in the previous subsection. The details of these reactions, such as the target nuclei used and incident energies, are listed in Table 2. The theoretical predicted single-nucleon removal cross sections using the NTG and the OLA, σ_{-1N}^{NTG} and σ_{-1N}^{OLA}, respectively, are also listed together with the experimental single-nucleon removal

Table 2 Experimental (σ_{-1N}^{exp}) and theoretical inclusive single-nucleon removal cross sections calculated with the OLA (σ_{-1N}^{OLA}) and the NTG model (σ_{-1N}^{NTG}), and the corresponding reduction factors $\mathfrak{R}^{OLA}$ and $\mathfrak{R}^{NTG}$

Reaction	ΔS_{eff} (MeV)	Target	E_{inc} (MeV/u)	σ_{-1N}^{exp} (mb)	σ_{-1N}^{OLA} (mb)	σ_{-1N}^{NTG} (mb)	$\mathfrak{R}^{OLA}$	$\mathfrak{R}^{NTG}$
(^{20}C,^{19} C)	– 26.574	C	240	58(5) [51]	47.55	51.88	1.22(11)	1.12(10)
(^{19}C,^{18} C)	– 24.142	Be	57	264(80) [52]	179.06	201.62	1.47(45)	1.31(40)
	– 24.104	Be	64	226(65) [53]	176.69	195.48	1.28(37)	1.16(33)
	– 23.754	C	243	163(12) [51]	134.75	146.63	1.21(9)	1.11(8)
Average	– 24.022						1.22(8)	1.12(8)
(^{18}C,^{17} C)	– 21.793	C	43	115(18) [49]	103.20	128.70	1.11(17)	0.89(14)
(^{17}C,^{16} C)	– 20.130	C	49	84(8) [49]	92.80	109.70	0.91(9)	0.77(7)
	– 20.121	Be	62	115(14) [52]	87.80	100.77	1.31(16)	1.14(14)
	– 20.121	Be	79	116(18) [54]	90.37	100.48	1.28(20)	1.15(18)
Average	– 20.124						1.03(7)	0.88(6)
(^{15}C,^{14} C)	– 18.275	C	54	137(16) [49]	180.56	196.44	0.76(9)	0.70(8)
	– 18.242	C	62	159(15) [49]	176.11	189.78	0.90(8)	0.84(8)
	– 18.169	C	83	146(23) [36]	166.44	176.08	0.88(14)	0.83(13)
	– 17.879	Be	103	146(23) [53]	142.52	149.89	0.98(3)	0.94(3)
Average	– 18.155						0.95(3)	0.90(0)
(^{16}C,^{15} C)	– 18.055	C	55	65(6) [49]	90.90	103.73	0.72(7)	0.63(6)
	– 18.053	C	62	77(9) [49]	89.78	101.10	0.86(10)	0.76(9)
	– 18.045	Be	75	81(7) [50]	81.99	90.94	0.99(9)	0.89(8)
	– 18.094	C	83	65(5) [52]	86.75	94.87	0.75(6)	0.69(5)
Average	– 18.051						0.80(4)	0.71(3)
(^{14}C,^{13} C)	– 10.807	C	67	65(4) [49]	133.284	148.61	0.49(3)	0.44(3)
	– 10.800	C	83	67(14) [36]	130.74	142.66	0.51(13)	0.47(12)
	– 10.767	C	235	80(7) [55]	110.92	121.39	0.72(6)	0.66(6)
Average	– 10.793						0.53(3)	0.48(2)
(^{12}C,^{11} C)	3.259	C	95	53(22) [56]	102.21	111.06	0.52(22)	0.48(20)
	3.266	C	240	60.51(11.08) [57]	94.12	104.37	0.64(12)	0.58(11)
	3.265	C	250	56.0(41) [58]	93.73	104.31	0.60(4)	0.54(4)
Average	3.263						0.60(4)	0.54(4)
(^{10}C,^{9} C)	17.277	Be	120	23.4(11) [59]	47.40	51.65	0.49(2)	0.45(2)
	17.277	C	120	27.4(13) [59]	49.72	54.36	0.55(3)	0.50(2)
Average	17.277						0.52(2)	0.48(2)
(^{9}C,^{8} B)	– 12.925	Be	67	48.6(73) [60]	62.77	66.67	0.77(12)	0.73(11)
	– 12.925	Be	100	56(3) [61]	58.77	59.72	0.95(5)	0.94(5)
Average	– 12.925						0.92(5)	0.90(5)
(^{12}C,^{11} B)	– 2.237	C	230	63.9(66) [62]	103.75	105.33	0.62(6)	0.61(6)
	– 2.237	C	250	65.6(26) [58]	102.93	105.36	0.64(3)	0.62(2)
Average	– 2.237						0.63(2)	0.62(2)
(^{13}C,^{12} B)	13.523	C	234	39.5(60) [62]	79.69	81.55	0.43(5)	0.40(4)
(^{14}C,^{13} B)	12.830	C	235	41.3(27) [62]	78.65	81.43	0.53(3)	0.51(3)
(^{16}C,^{15} B)	18.303	Be	75	18(2) [50]	60.23	62.50	0.30(3)	0.29(3)
	18.303	Be	239	16(2) [63]	56.86	58.45	0.28(4)	0.27(3)
	18.303	C	239	18(2) [62]	54.57	55.87	0.33(4)	0.32(4)
Average	18.303						0.30(2)	0.28(2)
(^{15}C,^{14} B)	20.134	C	237	28.4(28) [62]	55.36	57.58	0.51(5)	0.49(5)

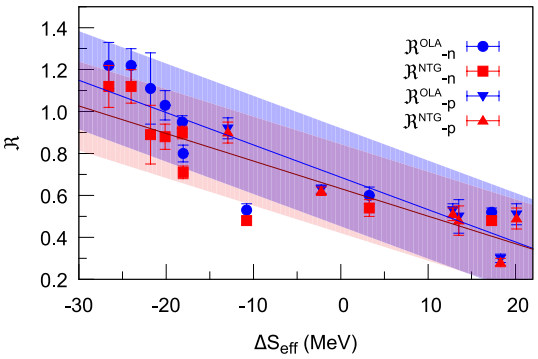

Fig. 4 (Color online) Averaged reduction factors $\mathfrak{R}$ listed in Table 2 as functions of the effective neutron–proton asymmetry $\Delta S_{\rm eff}$. The red squares and blue dots are results of the neutron removal of the NTG model and the OLA, respectively. The red triangles and blue inverted triangles are the same but for proton removal. The light red and blue bands represent the widths of their distributions

cross sections, $\sigma_{-1\rm N}^{\rm exp}$, and the reduction factors, $\mathfrak{R}^{\rm NTG}$ and $\mathfrak{R}^{\rm OLA}$, respectively. The single-particle spectroscopic factors (C^2S) used in these calculations were obtained from references corresponding to the experimental data and Ref. [47]. The reduction factors are presented in Fig. 4 as functions of neutron–proton asymmetry. Because many $\sigma_{-1\rm N}$ were measured inclusively, that is, they include all bound states of the core nuclei, which correspond to different separation energies of the removed nucleon, an effective neutron–proton asymmetry is used here: $\Delta S_{\rm eff} = S_{\rm n} + \bar{E}_{\rm f} - S_{\rm p}$ for neutron removal and $\Delta S_{\rm eff} = S_{\rm p} + \bar{E}_{\rm f} - S_{\rm n}$ for proton removal, where $\bar{E}_{\rm f}$ is the weighted mean excitation energy of the core nucleus, $\bar{E}_{\rm f} = \left(\sum_i E_{{\rm ex},i}\sigma_{{\rm sp},i}\right)/\sum_i \sigma_{{\rm sp},i}$, with $E_{{\rm ex},i}$ and $\sigma_{{\rm sp},i}$ being the excitation energy of the core nucleus in its i-th state and the corresponding single-particle cross section with Eq. (21) [11]. In all these calculations, the single-particle wave functions are calculated with Woods–Saxon potentials whose radius parameters, r_0, are determined with the HF calculations [48] and the diffuseness parameters being fixed as $a = 0.65$ fm except for the ^{15,17,18}C projectiles, for which the $r_0 = 1.15$ fm and $a = 0.50$ fm are used following Ref. [49]. And for proton removal of ^{16}C, $r_0 = 1.40$ fm and $a = 0.70$ fm are used following Ref. [50]. The proton and neutron density distributions of the nucleus ^{9}Be are taken to be a Gaussian form with a root mean square radius of 2.36 fm [12].

As shown in Table 2, $\sigma_{-1\rm N}$ values predicted with the NTG model are generally larger than those predicted with the OLA. Thus, the $\mathfrak{R}$ values with the NTG are smaller than those with the OLA. On average, the changes in the $\mathfrak{R}$ values induced by the NTG model with respect to the OLA are approximately 7.8%. However, as shown in Fig. 4, the $\mathfrak{R}$ values with the NTG model and the OLA, $\mathfrak{R}^{\rm NTG}$ and $\mathfrak{R}^{\rm OLA}$, respectively, still depend linearly on the effective neutron–proton asymmetry $\Delta S_{\rm eff}$, although the slope with the NTG model is 18% smaller than that with the OLA. The parameters of this linear dependence are

$$\begin{aligned}\mathfrak{R}^{\rm OLA} &= 0.687 - 0.0154\Delta S_{\rm eff},\\ \mathfrak{R}^{\rm NTG} &= 0.633 - 0.0131\Delta S_{\rm eff}.\end{aligned} \tag{24}$$

Thus, the systematics of the $\mathfrak{R}$ values with respect to $\Delta S_{\rm eff}$ observed in Refs. [11, 12] persist even when the multiple scattering effects inherited in the NTG model are included in the Glauber model calculations.

A closer examination of Fig. (4) shows that the differences between $\mathfrak{R}^{\rm NTG}$ and $\mathfrak{R}^{\rm OLA}$ in the most negative $\Delta S_{\rm eff}$ region are larger than those in the most positive $\Delta S_{\rm eff}$ region. Specifically, the average differences between $\mathfrak{R}^{\rm NTG}$ and $\mathfrak{R}^{\rm OLA}$ are 9.9% for $\Delta S_{\rm eff} < -10$ MeV and 5.3% for $\Delta S_{\rm eff} > 10$ MeV. This suggests that the multiple scattering effect introduced by the NTG model is more important for the removal of weakly bound nucleons than for deeply bound nucleons. This is misleading. Most cases in the $\Delta S_{\rm eff} < -10$ MeV region are single-neutron removal reactions and those in the $\Delta S_{\rm eff} > 10$ MeV region are single-proton removal reactions. From the $\mathfrak{R}^{\rm NTG}$ and $\mathfrak{R}^{\rm OLA}$ values listed in Table 2, it is clear that the average differences between $\mathfrak{R}^{\rm NTG}$ and $\mathfrak{R}^{\rm OLA}$ are 10.6% and 4.2% for neutron and proton removal reactions, respectively. Currently, it is unclear why the NTG model exhibits such systematic differences in these two types of reactions. As discussed at the end of the previous section, the only difference between the NTG model and the OLA is in the core–target S-matrices, $S_{\rm c}$. However, as expressed in Eqs. (18) and (19), $S_{\rm c}$ cannot be separated from $S_{\rm v}$ and the single-particle wave functions when calculating the single-nucleon removal cross sections. This implies that the multiple scattering effects induced in the NTG model on $\sigma_{-1\rm N}$ through $S_{\rm c}$ are moderated by single-particle wave functions, which are different for different cases. Therefore, we cannot explicitly show how the NTG model alone affects the $\sigma_{-1\rm N}$ values or why it behaves differently for proton and neutron removal reactions.

4 Summary

The reduction in single-particle strengths, represented by the reduction factors of single-nucleon spectroscopic factors extracted from experimental data with respect to the configuration interaction shell model predictions, is supposed to be related to the nucleon–nucleon correlations in atomic nuclei. Much theoretical and experimental effort has been devoted to this field of research. One of the open questions is why the reduction factors obtained from intermediate- and high-energy single-nucleon removal

cross sections such as those compiled in Refs. [11, 12] show strong linear dependence on the neutron–proton asymmetry, whereas those of other types of reactions, such as (p, pN) and single-nucleon transfer reactions, do not [2, 3, 6, 9, 64, 65]. Because single-nucleon removal reactions were analyzed using the Glauber model, the validity of the Glauber model for such reactions is questioned. In this respect, corrections to the Glauber model and an examination of their effects on single-nucleon removal cross sections are important.

In this study, we examined how the nucleon–target version of the Glauber model (the NTG model), which introduces multiple scattering of the constituent nucleons in the projectile and the target nuclei, can change the theoretically predicted single-nucleon removal cross sections with respect to the usual optical limit approximation, which does not contain multiple scattering effects. For this purpose, we first examined the NTG model in its reproduction of the elastic scattering angular distributions and the total reaction cross sections of the ^{12}C + ^{12} C system and compared their results with the experimental data and those calculated with the OLA. The NTG model was found to improve the description of the elastic scattering angular distributions, particularly at lower incident energies. Both the elastic scattering and total reaction cross sections calculated in this work agree well with those reported in previous publications, for example, Refs. [21, 23, 30].

We then compared the predictions of the inclusive single-nucleon removal cross sections using the NTG model and OLA. The case studied is the ^{9}Be(^{19}C, ^{18}C)X reaction within the incident energy range from 64 MeV/u to 400 MeV/u. The σ_{-1n} values predicted by the NTG model were larger than those predicted by the OLA within the entire energy range. This difference is larger at lower incident energies. It is also larger when the separation energy of the nucleon is larger, which corresponds to a smaller root mean square radius of the single-particle wave function.

Finally, we studied the extent to which the reduction factors of the single-particle strengths obtained from single-nucleon removal reactions changed when the NTG model was used instead of the OLA. The cases studied are one-nucleon removal reactions induced by $^{9,10,12-20}$C isotopes on carbon and ^{9}Be targets. On average, the reduction factors obtained with the NTG model were found to be less than those obtained with the OLA by 7.8%. We also found that the average differences in σ_{-1n} are larger than those in σ_{-1p} by 10.6% and 4.2%. However, the linear dependence of the reduction factor on the neutron–proton asymmetry persisted. Thus, the question of why the reduction factors of the single-particle strengths from single-nucleon removal reaction measurements depend differently on ΔS with respect to other types of reactions remains open, even when the multiple scattering effect is included in the Glauber model analysis with the NTG model.

Acknowledgements We thank Profs. J.A. Tostevin and W. Horiuchi for their help during this work.

Author Contributions All authors contributed to the study conception and design. Material preparation, data collection, and theoretical analysis were performed by Rui-Ying Chen, Yi-Ping Xu, Cen-Xi Yuan, and Wen-Long Hai. The first draft of the manuscript was written by Rui-Ying Chen and Dan-Yang Pang, and all authors commented on previous versions of the manuscript. All authors read and approved the final manuscript.

Data Availability The data that support the findings of this study are openly available in Science Data Bank at https://cstr.cn/31253.11.sciencedb.j00186.00648 and https://doi.org/10.57760/sciencedb.j00186.00648.

Declarations

Conflict of interest Cen-Xi Yuan is an editorial board member for Nuclear Science and Techniques and was not involved in the editorial review, or the decision to publish this article. All authors declare that there is no conflict of interest.

References

1. N.K. Glendenning, *Direct Nuclear Reactions* (World Scientific, Singapore, 2004), pp.89–106
2. B.P. Kay, J.P. Schiffer, S.J. Freeman, Quenching of cross sections in nucleon transfer reactions. Phys. Rev. Lett. **111**, 042502 (2013). https://doi.org/10.1103/PhysRevLett.111.042502
3. B.P. Kay, T.L. Tang, I.A. Tolstukhin et al., Quenching of single-particle strength in $A = 15$ nuclei. Phys. Rev. Lett. **129**, 152501 (2022). https://doi.org/10.1103/PhysRevLett.129.152501
4. V.R. Pharipe, I. Sick, P.KAd. Huberts, Independent particle motion correlations in fermion systems. Rev. Mod. Phys. **69**, 981–991 (1997). https://doi.org/10.1103/RevModPhys.69.981
5. W. Dickhoff, C. Barbieri, Self-consistent green's function method for nuclei nuclear matter. Progress Particle Nucl. Phys. **52**, 377–496 (2004). https://doi.org/10.1016/j.ppnp.2004.02.038
6. Y.P. Xu, D.Y. Pang, X.Y. Yun et al., Proton-neutron asymmetry independence of reduced single-particle strengths derived from (p, d)reactions. Phys. Lett. B **790**, 308 (2019). https://doi.org/10.1016/j.physletb.2019.01.034
7. W. Liu, J.L. Lou, Y.L. Ye et al., Experimental study of intruder components in light neutron-rich nuclei via single-nucleon transfer reaction. Nucl. Sci. Tech. **31**, 20 (2020). https://doi.org/10.1007/s41365-020-0731-y
8. S.L. Chen, Z.X. Liu, Z. Zhang et al., Systematic investigation of nucleon optical model potentials in (p, d) transfer reactions. Chin. Phys. C **48**, 074104 (2024). https://doi.org/10.1088/1674-1137/ad4269
9. L. Atar, S. Paschalis, C. Barbieri et al., Quasifree (p, $2p$) reactions on oxygen isotopes: observation of isospin independence of the reduced single-particle strength. Phys. Rev. Lett. **120**, 052501 (2018). https://doi.org/10.1103/PhysRevLett.120.052501
10. F. Flavigny, N. Keeley, A. Gillibert et al., Single-particle strength from nucleon transfer in oxygen isotopes: sensitivity to model parameters. Phys. Rev. C **97**, 034601 (2018). https://doi.org/10.1103/PhysRevC.97.034601

11. J.A. Tostevin, A. Gade, Systematics of intermediate-energy single-nucleon removal cross sections. Phys. Rev. C **90**, 057602 (2014). https://doi.org/10.1103/PhysRevC.90.057602
12. J.A. Tostevin, A. Gade, Updated systematics of intermediate-energy single-nucleon removal cross sections. Phys. Rev. C **103**, 054610 (2021). https://doi.org/10.1103/PhysRevC.103.054610
13. P. Hansen, J. Tostevin, Direct reactions with exotic nuclei. Ann. Rev. Nucl. Particle Sci. **53**, 219–261 (2003). https://doi.org/10.1146/annurev.nucl.53.041002.110406
14. T. Pohl, Y.L. Sun, A. Obertelli et al., Multiple mechanisms in proton-induced nucleon removal at ∼ 100 MeV/Nucleon. Phys. Rev. Lett. **130**, 172501 (2023). https://doi.org/10.1103/PhysRevLett.130.172501
15. E.C. Simpson, J.A. Tostevin, One- two-neutron removal from the neutron-rich carbon isotopes. Phys. Rev. C **79**, 024616 (2009). https://doi.org/10.1103/PhysRevC.79.024616
16. C. Bertulani, Core destruction in knockout reactions. Phys. Lett. B **846**, 138250 (2023). https://doi.org/10.1016/j.physletb.2023.138250
17. M.Q. Ding, D.Q. Fang, Y.G. Ma, Neutron skin and its effects in heavy-ion collisions. Nucl. Sci. Tech. **35**, 211 (2024). https://doi.org/10.1007/s41365-024-01584-1
18. Y.H. Wang, D.Y. Pang, W.D. Chen et al., Nuclear radii from total reaction cross section measurements at intermediate energies with complex turning point corrections to the eikonal model. Phys. Rev. C **109**, 014621 (2024). https://doi.org/10.1103/PhysRevC.109.014621
19. J.F. Wang, H.J. Xu, F.Q. Wang, Impact of initial fluctuations and nuclear deformations in isobar collisions. Nucl. Sci. Tech. **35**, 108 (2024). https://doi.org/10.1007/s41365-024-01480-8
20. Y. Suzuki, K. Yabana, R.G. Lovas et al., *Structure Reactions of Light Exotic Nuclei* (Taylor & Francis, Milton Park, 2003)
21. B. Abu-Ibrahim, Y. Suzuki, Scatterings of complex nuclei in the Glauber model. Phys. Rev. C **62**, 034608 (2000). https://doi.org/10.1103/PhysRevC.62.034608
22. B. Abu-Ibrahim, Y. Suzuki, Utility of nucleon-target profile function in cross section calculations. Phys. Rev. C **61**, 051601 (2000). https://doi.org/10.1103/PhysRevC.61.051601
23. W. Horiuchi, Y. Suzuki, B. Abu-Ibrahim et al., Systematic analysis of reaction cross sections of carbon isotopes. Phys. Rev. C **76**, 044607 (2007). https://doi.org/10.1103/PhysRevC.75.044607
24. R.J. Glauber, *in Lectures on Theoretical Physics* (Interscience, New York, 1959)
25. S. Hatakeyama, S. Ebata, W. Horiuchi et al., Multiple-scattering effects in proton- and alpha-nucleus reactions with Glauber theory. J. Phys. Conf. Ser. **569**, 012050 (2014). https://doi.org/10.1088/1742-6596/569/1/012050
26. L. Ray, Proton-nucleus total cross sections in the intermediate energy range. Phys. Rev. C **20**, 1857–1872 (1979). https://doi.org/10.1103/PhysRevC.20.1857
27. C. Werneth, X. Xu, R. Norman et al., Validation of elastic cross section models for space radiation applications. Nucl. Instrum. Meth. Phys. Res. Sect. B **392**, 74–93 (2017). https://doi.org/10.1016/j.nimb.2016.12.009
28. R.L. Workman, V.D. Burkert, V. Crede et al., Review of particle physics. PTEP **2022**, 083C01 (2022). https://doi.org/10.1093/ptep/ptac097
29. J.A. Tostevin, Cross sections of removal reactions populating weakly-bound residual nuclei (2022). https://doi.org/10.48550/arXiv.2203.06058. arXiv:2203.06058
30. T. Nagahisa, W. Horiuchi, Examination of the ^{22}C radius determination with interaction cross sections. Phys. Rev. C **97**, 054614 (2018). https://doi.org/10.1103/PhysRevC.97.054614
31. C. Bertulani, A. Gade, Momdis: a Glauber model computer code for knockout reactions. Comput. Phys. Commun. **175**, 372–380 (2006). https://doi.org/10.1016/j.cpc.2006.04.006
32. J. Hostachy, M. Buenerd, J. Chauvin et al., Elastic inelastic scattering of ^{12}C ions at intermediate energies. Nucl. Phys. A **490**, 441–470 (1988). https://doi.org/10.1016/0375-9474(88)90514-3
33. M. Buenerd, A. Lounis, J. Chauvin et al., Elastic inelastic scattering of carbon ions at intermediate energies. Nucl. Phys. A **424**, 313–334 (1984). https://doi.org/10.1016/0375-9474(84)90186-6
34. J.A. Tostevin, M.H. Lopes, R.C. Johnson, Elastic scattering and deuteron-induced transfer reactions. Nucl. Phys. A **465**, 83–122 (1984). https://doi.org/10.1016/0375-9474(87)90300-9
35. M. Takechi, M. Fukuda, M. Mihara et al., Reaction cross sections at intermediate energies and Fermi-motion effect. Phys. Rev. C **79**, 061601(R) (2009). https://doi.org/10.1103/PhysRevC.79.061601
36. D.Q. Fang, T. Yamaguchi, T. Zheng et al., One-neutron halo structure in ^{15}C. Phys. Rev. C **69**, 034613 (2004). https://doi.org/10.1103/PhysRevC.69.034613
37. S. Kox, A. Gamp, C. Perrin et al., Trends of total reaction cross sections for heavy ion collisions in the intermediate energy range. Phys. Rev. C **35**, 1678–1691 (1987). https://doi.org/10.1103/PhysRevC.35.1678
38. J. Jaros, A. Wagner, L. Erson et al., Nucleus-nucleus total cross sections for light nuclei at 1.55 2.89 GeV/*c* per nucleon. Phys. Rev. C **18**, 2273–2292 (1978). https://doi.org/10.1103/PhysRevC.18.2273
39. T. Zheng, T. Yamaguchi, A. Ozawa et al., Study of halo structure of ^{16}C from reaction cross section measurement. Nucl. Phys. A **709**, 103–118 (2002). https://doi.org/10.1016/S0375-9474(02)01043-6
40. H. Zhang, W. Shen, Z. Ren et al., Measurement of reaction cross section for proton-rich nuclei (A<30) at intermediate energies. Nucl. Phys. A **707**, 303–324 (2002). https://doi.org/10.1016/S0375-9474(02)01007-2
41. C. Perrin, S. Kox, N. Longequeue et al., Direct measurement of the ^{12}C +^{12} C reaction cross section between 10 83 MeV/nucleon. Phys. Rev. Lett. **49**, 1905–1909 (1982). https://doi.org/10.1103/PhysRevLett.49.1905
42. M. Takechi, M. Fukuda, M. Mihara et al., Reaction cross-sections for stable nuclei nucleon density distribution of proton drip-line nucleus 8B. Eur. Phys. J. A **25**, 217–219 (2005). https://doi.org/10.1140/epjad/i2005-06-078-0
43. L. Ponnath, T. Aumann, C. Bertulani et al., Measurement of nuclear interaction cross sections towards neutron-skin thickness determination. Phys. Lett. B **855**, 138780 (2024). https://doi.org/10.1016/j.physletb.2024.138780
44. D.T. Khoa, α-nucleus optical potential in the double-folding model. Phys. Rev. C **63**, 034007 (2018). https://doi.org/10.1103/PhysRevC.63.034007
45. K. Hencken, G. Bertsch, H. Esbensen, Breakup reactions of the halo nuclei ^{11}Be^{8}B. Phys. Rev. C **54**, 3043–3050 (1996). https://doi.org/10.1103/PhysRevC.54.3043
46. A.E.L. Dieperink, T. de Forest, Center-of-mass effects in single-nucleon knock-out reactions. Phys. Rev. C **10**, 543 (1974). https://doi.org/10.1103/PhysRevC.10.543
47. Y.P. Xu, D.Y. Pang, C.X. Yuan et al., Quenching of single-particle strengths of carbon isotopes $^{9-12,14-20}$C with knockout reactions for incident energies 43–2100 Mev/nucleon *. Chin. Phys. C **46**, 064102 (2022). https://doi.org/10.1088/1674-1137/ac5236
48. W.L. Hai, D.Y. Pang, X.B. Wang et al., Determining the radii of single-particle potentials with Skyrme Hartree-Fock calculations. Phys. Rev. C **110**, 044613 (2024). https://doi.org/10.1103/PhysRevC.110.044613

49. E. Sauvan, F. Carstoiu, N.A. Orr et al., One-neutron removal reactions on light neutron-rich nuclei. Phys. Rev. C **69**, 044603 (2004). https://doi.org/10.1103/PhysRevC.69.044603
50. F. Flavigny, A. Obertelli, A. Bonaccorso et al., Nonsudden limits of heavy-ion induced knockout reactions. Phys. Rev. Lett. **108**, 252501 (2012). https://doi.org/10.1103/PhysRevLett.108.252501
51. N. Kobayashi, T. Nakamura, J.A. Tostevin et al., One-two-neutron removal reactions from the most neutron-rich carbon isotopes. Phys. Rev. C **86**, 054604 (2012). https://doi.org/10.1103/PhysRevC.86.054604
52. V. Maddalena, T. Aumann, D. Bazin et al., Single-neutron knockout reactions: application to the spectroscopy of ^{16,17,19}C. Phys. Rev. C **63**, 024613 (2001). https://doi.org/10.1103/PhysRevC.63.024613
53. J.R. Terry, D. Bazin, B.A. Brown et al., Absolute spectroscopic factors from neutron knockout on the halo nucleus ^{15}C. Phys. Rev. C **69**, 054306 (2004). https://doi.org/10.1103/PhysRevC.69.054306
54. C. Wu, Y. Yamaguchi, A. Ozawa et al., Neutron removal reactions of ^{17}C. J. Phys. G. Nucl. Partic. **31**, 39 (2004). https://doi.org/10.1088/0954-3899/31/1/004
55. Y.Z. Sun, S.T. Wang, Z.Y. Sun et al., Single-neutron removal from ^{14,15,16}C near 240 MeV/nucleon. Phys. Rev. C **104**, 014310 (2021). https://doi.org/10.1103/physrevc.104.014310
56. J. Dudouet, D. Juliani, M. Labalme et al., Double-differential fragmentation cross-section measurements of 95 MeV/nucleon ^{12}C beams on thin targets for hadron therapy. Phys. Rev. C **88**, 024606 (2013). https://doi.org/10.1103/PhysRevC.88.024606
57. Y. Sun, Y. Zhao, S. Jin et al., Data analysis framework for radioactive ion beam experiments at the external target facility of HIRFL-CSR. Nucl. Phys. Rev. **37**, 742 (2020). https://doi.org/10.11804/NuclPhysRev.37.2019CNPC27
58. B.A. Brown, G. Hansen, B.M. Sherrill et al., Absolute spectroscopic factors from nuclear knockout reactions. Phys. Rev. C **65**, 061601 (2002). https://doi.org/10.1103/PhysRevC.65.061601
59. G.F. Grinyer, D. Bazin, A. Gade et al., Systematic study of *p*-shell nuclei via single-nucleon knockout reactions. Phys. Rev. C **86**, 024315 (2012). https://doi.org/10.1103/PhysRevC.86.024315
60. R.J. Charity, L.G. Sobotka, J.A. Tostevin, Single-nucleon knockout cross sections for reactions producing resonance states at or beyond the drip line. Phys. Rev. C **102**, 044614 (2020). https://doi.org/10.1103/PhysRevC.102.044614
61. D. Bazin, R.J. Charity, R.T. de Souza et al., Mechanisms in knockout reactions. Phys. Rev. Lett. **102**, 232501 (2009). https://doi.org/10.1103/PhysRevLett.102.232501
62. Y.Z. Sun, S.T. Wang, Z.Y. Sun et al., One-proton removal from neutron-rich carbon isotopes in $^{12-16}$C beams near 240 MeV/nucleon beam energy. Phys. Rev. C **110**, 014603 (2024). https://doi.org/10.1103/PhysRevC.110.014603
63. Y.X. Zhao, Y.Z. Sun, S.T. Wang et al., One-proton knockout from ^{16}C at around 240 MeV/nucleon. Phys. Rev. C **100**, 044609 (2019). https://doi.org/10.1103/PhysRevC.100.044609
64. F. Flavigny, A. Gillibert, L. Nalpas et al., Limited asymmetry dependence of correlations from single nucleon transfer. Phys. Rev. Lett. **110**, 122503 (2013). https://doi.org/10.1103/PhysRevLett.110.122503
65. M. Gómez-Ramos, A. Moro, Binding-energy independence of reduced spectroscopic strengths derived from (p, 2p) (p, pn) reactions with nitrogen oxygen isotopes. Phys. Lett. B **785**, 511–516 (2018). https://doi.org/10.1016/j.physletb.2018.08.058